Research Article Vol. 3, No. 6 / 15 June 2020 / OSA Continuum 1703
OSA CONTINUUM

Large-size updatable optically addressed spatial light modulator (OASLM) based on ZnO nanoparticles for large-area holographic 3D displays

PAWAN KUMAR SHRESTHA,[1,3] XIN CHANG,[1,3] MATTHEW PRYN,[1] JIN LI,[1] GIRISH RUGHOOBUR,[2] KUN LI,[1] KASIA SUROWIECKA,[1] AND DAPING CHU[1,*]

[1] *Centre for Photonic Devices and Sensors, Department of Engineering, University of Cambridge, 9 JJ Thomson Ave, Cambridge, CB3 0FF, UK*
[2] *Department of Electrical Engineering and Computer Science, Massachusetts Institute of Technology, 77 Massachusetts Ave, Cambridge, MA 02139, USA*
[3] *These authors contributed equally to this paper*
[*] *dpc31@cam.ac.uk*

Abstract: Optically addressed spatial light modulators (OASLMs) provide an appropriate solution for large-area and wide-viewing angle holographic displays because of the possibility of uploading holograms on it through tiling and with sub-micron diffraction feature sizes. A prototype with a large-size OASLM of 100 mm × 100 mm was fabricated using a solution-based deposition process for ZnO nanoparticles (NPs). ZnO NP-based OASLM is suitable for hologram tiling because of the extended charge carrier lifetime as a result of trap states in the ZnO NP layer annealed at a low temperature of 180°C, of which the activation energy was determined firstly by low-temperature measurements. Operating the ZnO NP OASLM in a DC driving mode was subsequently proposed, to utilize the extended charge carrier lifetime in the photosensor layer for temporary information storage. Finally, techniques to tile computer generated holograms (CGHs) spatially on a single OASLM were explored and evaluated, including the demonstration of simultaneous image replay from sequentially tiled two separate phase-only CGHs.

1. Introduction

Holographic displays are ideal to display three-dimensional (3D) images with all the accommodation depth cues. In an ideal case, there is no difference between the wavefront emitted by the real object or its hologram. However, it is challenging to show good quality and updatable 3D images of large area and wide viewing angles with rewritable holograms of sufficiently small pixel size and high enough resolution since it requires very high resolution with large pixel count. Current commercial SLMs are based on liquid crystal (LC), e.g. LC on silicon (LCOS) and digital micromirror devices (DMD), both of which have relatively small pixel sizes but also a limited viewing aperture. To overcome this challenge, multiple SLMs may be tiled spatially or angularly. However, building a seamless large hologram using such a method is still challenging and the system cost scales poorly.

Alternatively, a large-area high-resolution hologram can be created by tiling holographic patterns onto an optically addressed SLM (OASLM). QinetQ [1,2] used a method termed Active Tiling to achieve a very high pixel count using a high speed binary electrically addressed SLM (EASLM) as an image engine and a bi-stable ferroelectric LC based OASLM. The OASLM electrodes are lithographically patterned to exactly match the computer-generated hologram

#386258 https://doi.org/10.1364/OSAC.386258
Journal © 2020 Received 23 Dec 2019; revised 23 Apr 2020; accepted 23 Apr 2020; published 15 Jun 2020

OSA CONTINUUM

(CGH) segments displayed in the EASLM. Data generated by the EASLM is replicated at all segments of the OASLM, and then written on the desired segment of the OASLM using a shutter. The high resolution of an OASLM provides an opportunity to demagnify the pixel size of the image engine in order to increase the viewing angle of the hologram. However, the OASLM segments need to be addressed using passive matrix driving which inherently leaks a third of driving voltage to unselected neighboring segments.

Several attempts have been made to realize the hologram tiling such as using a single DMD device [3], multiple ferroelectric LCOS devices [4,5] and a two-dimensional scanner followed by an f-theta lens [6]. Tiling using an OASLM comprised of a-Si:H and ferroelectric LC for a cell with size ~5 cm × 5 cm has also been demonstrated by Cambridge University [7,8]. Other than spatial tiling where CGHs are normally partitioned and tiled spatially, angular tiling has been used to increase the viewing angle where tiled 3D scenes are tiled view by view [9,10]. Other attempts to enlarge the holographic image have also been reported [11–14]. The main difference between tiling with and without OASLM is that OASLM provides a platform for a complete CGH to be reconstructed, avoiding the need for each sub-hologram to be individually reconstructed.

In this paper, we use ZnO nanoparticle (NP) photosensor to fabricate a large area updatable OASLM with nematic LC. The ZnO NP layer in an OASLM configuration has been demonstrated to retain the information for ~10 s [15]. Contrary to storing holograms on LC layer, using a photosensor layer to store information does not require the OASLM to be segmented. Hence driving voltage can be applied to the whole cell and passive matrix addressing of the OASLM can be avoided. The solution-processed ZnO NPs can also easily be deposited over a large area. Nematic LCs only exhibit orientational order, making the LC alignment process significantly simpler compared to ferroelectric LCs. Furthermore, nematic LC exhibits an analogue response to an applied voltage. We propose a DC driving scheme with occasional resets for the OASLM and demonstrate it for tiling holograms for image reply.

2. Materials and methods

Generally, an OASLM is comprised of a 2D photosensor layer next to a light modulating layer between transparent conducting electrodes as depicted in Fig. 1(a). In this paper, we use solution-processed ZnO NPs as a photosensitive layer and nematic LCs as a light modulating layer to fabricate a large-size OASLM. The image of ZnO NPs taken by scanning electron microscopy (SEM) is shown in Fig. 1(b).

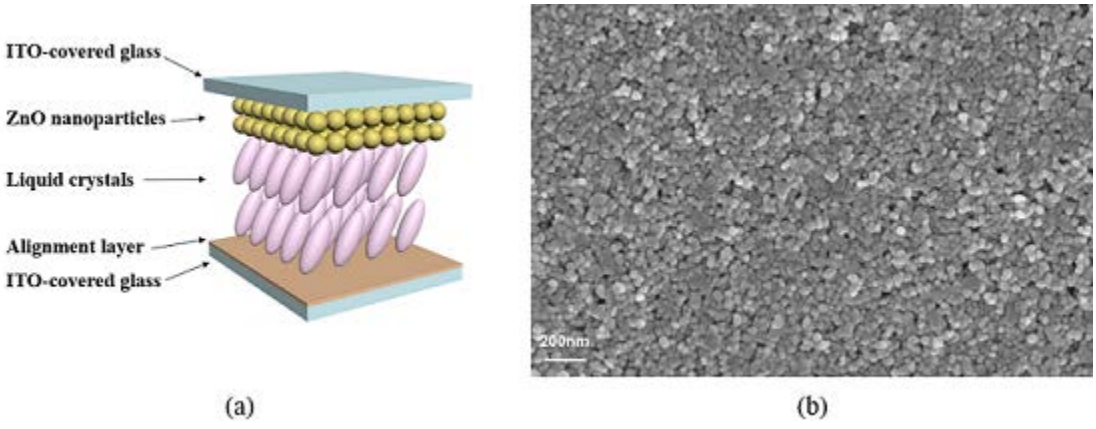

Fig. 1. (a) A typical structure of OASLM device; (b) SEM image of ZnO NPs.

OSA CONTINUUM

High-resolution holograms can be written on a ZnO NP-based OASLM due to the existence of trap states in ZnO NP. The trap states are also significant to the realization of hologram tiling. The tiling requires temporary storage of photogenerated charge carriers in photosensor layer and the storage time depends on the depth of trap states. The trap activation energy (Ea) of ZnO NP can be determined by Eq. (1):

$$\sigma = \sigma_0(e^{\left(\frac{Ea}{kT}\right)} \tag{1}$$

where σ is electrical conductivity and T is the measuring temperature. The constant σ0 is a function of charge carrier mobility and charge carrier density. The trap activation energy (Ea) is extracted by the slope of Arrhenius plot (1/T, log σ). Thin-film ZnO NP sample was prepared by spin-coating and aluminium (Al) electrodes (50 nm in thickness) were thermally deposited on top after thermal annealing at 400°C in air for 5h. Low-temperature IV measurement was carried out using a Lake Shore cryogenic probe station and Agilent 4156 (Yokogawa-Hewlett-Packard Ltd, Tokyo, Japan). The measuring temperature was cooled down by liquid nitrogen. The result is shown in Fig. 2(a).

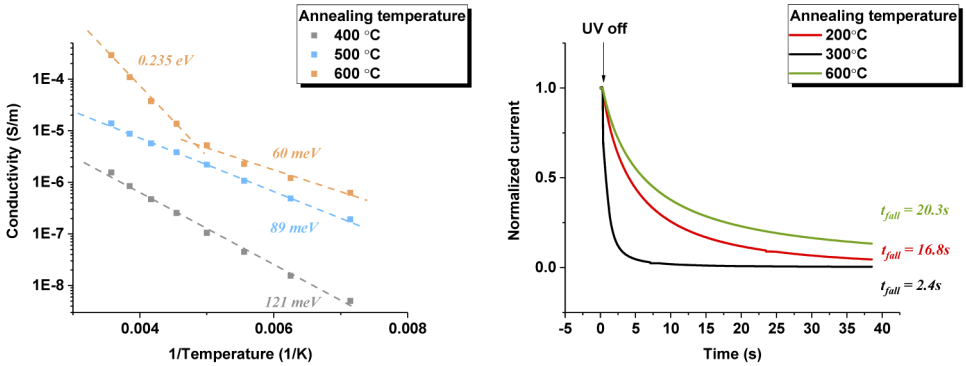

Fig. 2. (a) The Arrhenius plot of ZnO NP thin film annealed at 400°C, 500°C and 600°C. (b) The fall time of ZnO NP thin film annealed at 200°C, 300°C and 600°C.

It is evident from Fig. 2(a) that Ea for ZnO NP thin film annealed at 400°C is 121meV. Moreover, it has been reported that Ea can be modified by thermal annealing and a smaller Ea can be obtained by increasing the annealing temperature as a result of less impurities and better crystal quality [16,17]. This was verified by performing the same measurement on ZnO NP samples annealed at 500°C and 600°C, and Ea was determined to be 89 meV and 60 meV respectively, as is shown in Fig. 2(a). The effect of thermal annealing on Ea is also supported by comparing with published results. For instance, Ea of 0.278~0.321eV for single-crystal ZnO has been reported as a result of oxygen vacancies [18]. The Ea for dense sintered ZnO aggregate was also determined to be between 0.3~0.36eV [17]. In addition, it is also noticed that a deep trap state at 235meV is created by annealing at 600°C since new defects could be generated by high-temperature annealing [18–20]. The measurement of Ea for ZnO NP annealed at a lower temperature was not included here because the electrical conductivity is extremely low at low measurement temperature and the result was heavily affected by error. The photo response of ZnO NP thin film was also carried out, as is shown in Fig. 2(b). The fall time (current drops from 90% to 10%) was measured after UV was turned off and it clearly shows that the fall time was reduced from 16.8s to 2.4s by raising the annealing temperature from 200°C to 300°C. In the meanwhile, a longer fall time of 20.3s was observed at the annealing temperature of 600°C, indicating a deeper trap state produced at this temperature.

OSA CONTINUUM

Therefore it can be concluded that a lower annealing temperature is desirable for the application of hologram tiling. Hence the ZnO NP thin film was treated with reduced thermal annealing (180°C and 10 min) when fabricating the OASLM such that hologram tiling can be realized by charge trapping in ZnO NP layer. The detailed fabrication process is discussed in Section 3.

3. Experiments and results

The final OASLM devices used in this work for the hologram tiling test was 100 mm × 100 mm as shown in Fig. 3. ITO coated glass substrates were cleaned and spin-coated with the ZnO NP suspension in ethanol. The prepared thin films were annealed at 180 °C for 10 min in air. Polyimide (AM4276) was then spin-coated on a separate 100 mm × 100 mm glass substrate followed by annealing and rubbing. The cell was formed by gluing these two layers facing each other with 5.5 µm spacers. The rubbing direction of the alignment layer was aligned to the filling holes. The prepared cell was filled with E7 nematic LC by capillary effect. As the cell is large, care was taken to fill without trapping air bubbles.

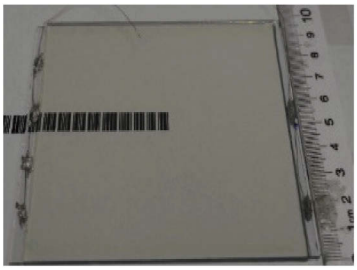

Fig. 3. The image of a 100 mm × 100 mm ZnO NP OASLM cell. A bar code is placed underneath the cell to demonstrate the transparency of the device.

A layer-based algorithm was used to calculate computer generated hologram (CGH) [15], as illustrated in Fig. 4, where a 3D object can be expressed as a set of 2D layers:

$$G(x, y, z) = F_z(x, y) \tag{2}$$

The layer images are Fourier transformed to create a holographic pattern for each layer:

$$P_z = \mathrm{FFT}(F_z(x, y)) \tag{3}$$

The holograms are then multiplied by a set of holographic lenses to allow the image plane to be reconstructed at its appropriate depth:

$$Q_z = P_z \times \exp\left[j\frac{k}{2}\left(\frac{x^2}{z_x} + \frac{y^2}{z_y}\right)\right] \tag{4}$$

where k is the wave number.

The hologram generated with the holographic lens combined becomes the final hologram for this view:

$$H = \sum\nolimits_z Q_z \tag{5}$$

In order to dynamically alter the holographic patterns, a DMD (V-9501 VIS Texas Instruments in the V4100 ViALUX development kit) was used. The DMD has a resolution of 1920 × 1080 and a pixel pitch of 10.8 µm. At the specified binary frame rate of 17 kHz, it can display 35.2 Giga pixel s^{-1}. We use 4f system to relay and de-magnify the image generated by the image engine. The first lens is placed at the distance of f1 (300 mm) from the image engine as shown

OSA CONTINUUM

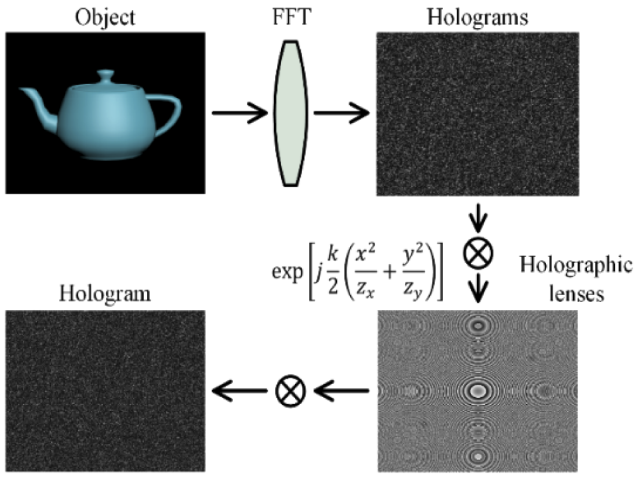

Fig. 4. Illustration of layer-based algorithm depicting generation of CGH.

in Fig. 5(a). The second lens is placed at the distance of (f1+f2) (450 mm) from the first lens. A demagnification of 0.5 was achieved by controlling the ratio of f1 and f2. A spatial filter at the Fourier plane can be used to remove the large angle diffraction orders generated by the pixellation of the image engine. A two-axis galvanometer scanner (Nutfield, USA) with ±12° optical scanning angle in both x and y axes was used to tile the sub holograms. In this work, galvo-scanner was only used to scan x-axis. However, when a galvo-scanner is used to write the

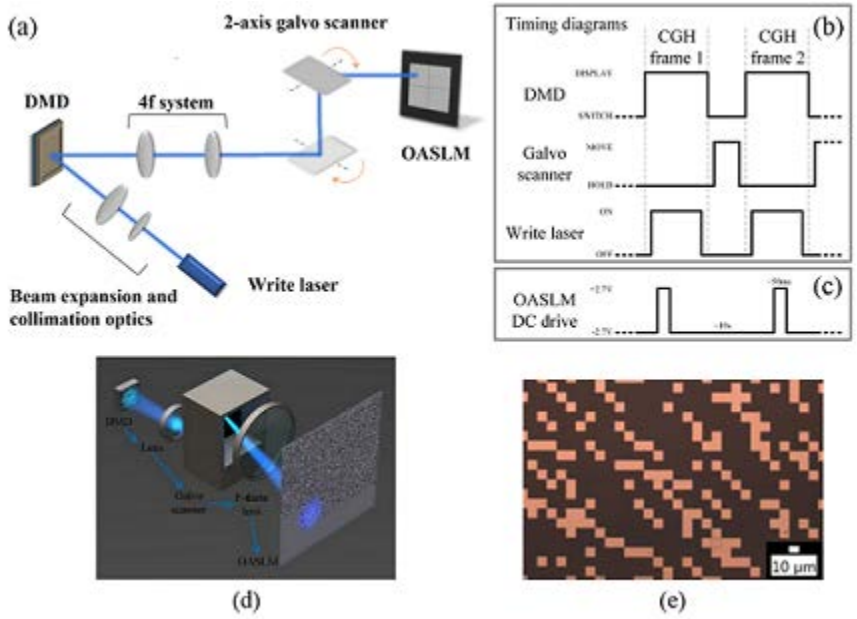

Fig. 5. (a) Experimental setup of tiling of OASLM with DMD as an image engine. (b) Timing diagrams of signals used to drive DMD, Galvo-scanner and write laser. (c) OASLM DC drive signal. (d) Illustration of the complete tiling system concept. (e) Microscope image of a CGH pattern fabricated using e-beam.

OSA CONTINUUM

image on different locations of the OASLM, the distance between the image plane and the lenses varies. This can be potentially corrected by replacing the second lens of the 4f system with an f-theta lens. Alternatively, the OASLM may be mounted on the mechanical stage and moved to write each new frame.

A CGH was displayed on the DMD for 2s illuminated by the 405 nm write laser. At the end of the frame, the laser was triggered to turn off for 100 ms while the galvo-scanner repositioned. A second frame of CGH was uploaded and written to the OASLM. Once both holograms were written, the replay field was created by illuminating the OASLM with 635 nm read light. The timing diagram and OASLM driving signals are shown in Figs. 5(b)–5(c). Synchronisation between the DMD and the galvo-scanner has not been fully optimised, so each CGH was only written once per cycle. Uploading n × n tiled CGHs on the DMD with a shorter write interval but with repeated exposures may yield a better result. The scanning mirrors introduce some geometric distortions which can be pre-compensated in the image generated by the image engine. Figure 5(d) shows the illustration of the complete tiling system. The OASLM was driven by applying a 2.7 V and pulse of opposite polarity every 10 s to reset the driving signal in order to prevent ion concentrations from growing. Figures 6(a)–6(e) depicts the images used to generate holograms and captured results is shown in Fig. 6(e). Spatial filters are used to suppress the zero order in the replay field. The reconstructed images shown in Fig. 6 proved that the tiling of holograms can be realized with OASLM using ZnO NP as photosensitive material.

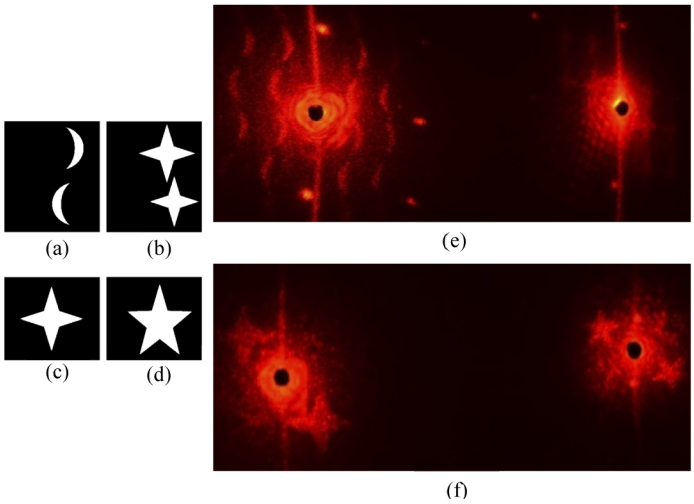

Fig. 6. (a-b) Patterns to form a CGH to be displayed by a DMD. (c-d) Patterns to form a CGH to be written by e-beam. (e) OASLM replay image of tiled holograms. DMD is used as an image engine. (f) OASLM replay image of tiled holograms. E-beam generated masks (with two different pixel sizes; hologram corresponding to Fig (c) of 8 µm pixel size and that of Fig (d) of 13 µm) are used as image sources. Images are optically demagnified by 0.5. Hence, the effective hologram pixel sizes on the OASLM are 4 and 6.5 µm respectively. Two different pixel sizes are used to demonstrate that OASLM can accommodate to different sizes simultaneously.

Higher replay quality was achieved by using a mask with hologram patterns, which was fabricated using e-beam lithography. 50 nm of ITO was coated on a cleaned borosilicate glass wafer with 500 ± 25 µm thickness by RF magnetron sputtering. Previously generated CGHs were converted into poly line using Matlab for ebeam processing. The substrate was spin-coated with ~350 nm UV1116 photoresist (Dow Chemical Company) followed by baking at 130°C for 2 min. E-beam lithography with a dose of 60 µC cm^{-2}, and a current of 5.1 nA at 80 kV, was

OSA CONTINUUM

used to write the 8–13 μm pixel size hologram over a 7 mm × 7 mm area. After exposure, the samples were post baked at 130°C for 2 min followed by development in MF-CD-26 for 30 s and rinsing with DI water followed by gentle blow dry with N_2 gas. The prepared samples were sputtered with 40 nm Aluminium by RF magnetron sputtering at a chamber pressure of 2×10^{-5} mbar. Lift off was performed by soaking samples in N-methyl-2-pyrrolidone (NMP) for 4 h followed by sonication in NMP, acetone, and IPA for ~15 s each and blow dried with N_2 gas. The final samples obtained through the process were binary amplitude modulated transmission hologram masks as shown in Fig. 5(e).

A motorized linear stage was used to switch between two masks whilst an optical system wrote the pattern onto an OASLM. The masks were mounted on the translational stage driven by a stepper motor. A write light (405nm) at 10 mW cm^{-2} was used to expose the OASLM through the mask for 2 s to write an image. Once the first hologram was recorded, write light was turned off for 500 ms while a galvo-scanner was triggered to change the write position, whilst the stepper motor was triggered to reveal the second hologram mask on the optical path. The second hologram was then written onto the OASLM under the same conditions. Once both holograms are written on the OASLM, two 635 nm lasers are used to replay the recorded holograms at ~2 mW cm^{-2}. A LabVIEW program was written to synchronize the write laser, galvo-scanner and stepper motor. The result is shown in Fig. 6(f). The replay quality can be further enhanced by improving the uniformity of ZnO NP and LC layer across the cell. In addition, the maximum size of OASLM is also affected by layer uniformity.

4. Conclusions

The characteristics of a large-size OASLM fabricated using solution-processed ZnO NPs together with nematic LCs have been studied in detail. A cryogenic analysis of trap activation energy of ZnO NP was conducted and it was found that lower annealing temperatures leads to deeper trap states. This results in a longer 'off' time for the OASLM, which can be used for holographic tiling. A large-area high-performance OASLM of 100 mm × 100 mm was fabricated at a relatively low temperature of 180°C and tested in a holographic display. Multiple holograms were written sequentially to the device in different areas using a scanning galvo-mirror system and 4f relay optics. The holograms were then replayed simultaneously. This could be extended by writing multiple sub-holograms to the same OASLM in a large-area high-resolution and updatable holographic display capable of delivering true 3D images with good image qualities and wide viewing angles.

Funding

Engineering and Physical Sciences Research Council (EP/L015455/1); China Scholarship Council.

Disclosures

The authors declare no conflicts of interest.

References

1. M. Stanley, P. B. Conway, S. D. Coomber, J. C. Jones, D. C. Scattergood, C. W. Slinger, R. W. Bannister, C. V. Brown, W. A. Crossland, and Adrian R. L. Travis, "Novel electro-optic modulator system for the production of dynamic images from giga-pixel computer-generated holograms," Proc. SPIE **3956**, 13–22 (2000).
2. M. Stanley, M. A. Smith, A. P. Smith, P. J. Watson, S. D. Coomber, C. D. Cameron, C. W. Slinger, and A. Wood, "3D electronic holography display system using a 100-megapixel spatial light modulator," Proc. SPIE **5249**, 297 (2004).
3. X. Xu, X. Liang, Y. Pan, R. Zheng, and Z. A. Lum, "Spatiotemporal multiplexing and streaming of hologram data for full-color holographic video display," Opt. Rev. **21**(3), 220–225 (2014).

OSA CONTINUUM

4. R. B. A. Tanjung, X. Xu, X. Liang, S. Solanki, Y. Pan, F. Farbiz, B. Xu, and T.-C. Chong, "Digital holographic three-dimensional display of 50-Mpixel holograms using a two-axis scanning mirror device," Opt. Eng. **49**(2), 025801 (2010).
5. H. Sasaki, K. Yamamoto, Y. Ichihashi, and T. Senoh, "Image size scalable full-parallax coloured three-dimensional video by electronic holography," Sci. Rep. **4**(1), 4000 (2015).
6. P. St-Hilaire, S. A. Benton, M. E. Lucente, and P. M. Hubel, "Color images with the MIT holographic video display," Proc. SPIE **1667**, 73–84 (1992).
7. H.-W. Jeon, A. R. L. Travis, N. Collings, T. D. Wilkinson, and Y. Frauel, "Image-tiling system using optically addressed spatial light modulator for high-resolution and multiview 3D display," Proc. SPIE **3957**, 165 (2000).
8. A. Henrie, J. R. Codling, S. Gneiting, J. B. Christensen, P. Awerkamp, M. J. Burdette, and D. E. Smalley, "Hardware and software improvements to a low-cost horizontal parallax holographic video monitor," Appl. Opt. **57**(1), A122 (2018).
9. F. Yaraş, H. Kang, and L. Onural, "Circular holographic video display system," Opt. Express **19**(10), 9147 (2011).
10. J. Jia, J. Chen, J. Yao, and D. Chu, "A scalable diffraction-based scanning 3D colour video display as demonstrated by using tiled gratings and a vertical diffuser," Sci. Rep. **7**(1), 44656 (2017).
11. K. Wakunami, P. Y. Hsieh, R. Oi, T. Senoh, H. Sasaki, Y. Ichihashi, M. Okui, Y. P. Huang, and K. Yamamoto, "Projection-type see-through holographic three-dimensional display," Nat. Commun. **7**(1), 12954 (2016).
12. N. Leister, A. Schwerdtner, G. Fütterer, S. Buschbeck, J.-C. Olaya, and S. Flon, "Full-color interactive holographic projection system for large 3D scene reconstruction," Proc. SPIE **6911**, 69110V (2008).
13. P. A. Blanche, A. Bablumian, R. Voorakaranam, C. Christenson, W. Lin, T. Gu, D. Flores, P. Wang, W. Y. Hsieh, M. Kathaperumal, B. Rachwal, O. Siddiqui, J. Thomas, R. A. Norwood, M. Yamamoto, and N. Peyghambarian, "Holographic three-dimensional telepresence using large-area photorefractive polymer," Nature **468**(7320), 80–83 (2010).
14. T. Kozacki, G. Finke, P. Garbat, W. Zaperty, and M. Kujawińska, "Wide angle holographic display system with spatiotemporal multiplexing," Opt. Express **20**(25), 27473 (2012).
15. P. K. Shrestha, Y. T. Chun, and D. Chu, "A high-resolution optically addressed spatial light modulator based on ZnO nanoparticles," Light: Sci. Appl. **4**(3), e259 (2015).
16. H. S. Kang, J. S. Kang, J. W. Kim, and S. Y. Lee, "Annealing effect on the property of ultraviolet and green emissions of ZnO thin films," J. Appl. Phys. **95**(3), 1246–1250 (2004).
17. Y. F. Lu, H. Q. Ni, Z. H. Mai, and Z. M. Ren, "The effects of thermal annealing on ZnO thin films grown by pulsed laser deposition," J. Appl. Phys. **88**(1), 498–502 (2000).
18. J. C. Simpson and J. F. Cordaro, "Characterization of deep levels in zinc oxide," J. Appl. Phys. **63**(5), 1781–1783 (1988).
19. Z. Q. Chen, S. Yamamoto, M. Maekawa, A. Kawasuso, X. L. Yuan, and T. Sekiguchi, "Postgrowth annealing of defects in ZnO studied by positron annihilation, x-ray diffraction, rutherford backscattering, cathodoluminescence, and Hall measurements," J. Appl. Phys. **94**(8), 4807–4812 (2003).
20. R. G. Singh, F. Singh, V. Kumar, and R. M. Mehra, "Growth kinetics of ZnO nanocrystallites: Structural, optical and photoluminescence properties tuned by thermal annealing," Curr. Appl. Phys. **11**(3), 624–630 (2011).